Numerical simulation of Power-Law inelastic fluid in channal by using finite element method

Reisan Y. Yasir, Alaa H. Al-Muslimawi
Department of Mathematics, College of Science
University of Basra

Doi 10.29072/basjs.20190202, Article inf., Received: 29/4/2019 Accepted: 13/6/2019 Published: 31/8/2019

Abstract

In this paper the numerical study for incompressible power-low inelastic fluid is presented. Physically, a continuity equation (mass conservation) and time-dependent conservation of momentum equations are utilized to describe the motion of the fluid. Moreover, the flow problem is solved under viscous inelastic assumptions, with a power-law inelastic model $(PLIM)$. Numerically, the study has been conducted based on the Galerkin finite element method $(GFEM)$. Attention is paid to the comparison between Newtonian results and shear-thinning inelastic.

The analysis of convergence under the parameters of power-low inelastic model and Reynolds number is conducted. The Findings reveal that, there is a significant effect from the inelastic parameters upon the the velocity temporal convergence-rates of velocity, while for pressue, the change in convergence is modest.

Keywords: Finite element method; Galerkin method; General Newtinian; Power low model

1 Introduction

In this study , a numereical analysis of inelastic (general Newtonian) fluid is performed with a Galerkin finit element ($GFEM$) algorithm. Here, the general Newtonian fluid is usually governed by two differential equations; named conservation of mass and time-dependent conservation of momentum. These equation are elliptic partial differential equations and presented in this investigation in cylindrical coordinate system (Axisymmetric flow) (for more detials see [1]).

Particularly, a general Newtonian fluid plays an important role in various industries, where many industrial processes involve this type of fluid. In this type of fluid the shear stress is defined as a non-linear function of shear rate at the particular time. So, we need to add a constitutive equation to treat the non-linearity behaviour of shear stress. For that purpose, power law shear-thinning (pseudo-plastic), shear thickness model is implemented as a well presented model for simulating this type of fluid. A power-law model is originally proposed by De Waele-Ostwald [2]. Also in 1929, Norton introduced a one-dimensional case of the power law [3]. In 1954, Hoff [4] proposed the power law in the three-dimensional version, and this model is named the Norton-Hoff one. This kind of model describes the shear stress as a function of a second invariant of rate of deformation tensor. Since this model contains two parameters only, thus one can say that this model is the easiest time-independent non Newtonian model [5]. Here, The ($PLIM$) is defined as ([6] , [7])

$$\tau = (k|\dot{\gamma}|^{n-1})\dot{\gamma},$$

where, $\dot{\gamma}$ is the shear rate for simple shear flow, k is a consistency parameter and n is a power-law index. Approximately, this viscosity model describes the behavior of a real non-Newtonian fluid. In the case of that ($n < 1$), the ($PLIM$) gives that the viscosity decreases as the shear rate increases, , which is called shear thinning liquid (more detials in sections 3 and 4 below). This case requires a fluid with infinite viscosity at rest and zero viscosity as the shear rate approaches infinity, but a real fluid has both a minimum and a maximum effective viscosity that depend on the physical chemistry at the molecular level. Therefore, the ($PLIM$) is only a good description of fluid behavior across the range of shear rates to which the coefficients were fitted. There are a number of other models that better describe the entire flow behavior of shear-dependent fluids, but they do so at the expense of simplicity, so the power law is still used to describe fluid behavior, permit mathematical predictions, and correlate experimental data.

Particularly, many studies have been done by using ($PLIM$). Garrioch and James [8] implemented

a numerical study for Newtonian and power-law shear-thinning fluids in high-speed, laminar flow through a conical channel. In this study, the study emphasized on the pressure drop of creeping Newtonian and Non-Newtonian flows in a cone. Missirlis et al. [9] studied the steady motion of spheres representing particles inside tubes filled with different fluids using both a finite-element and a finite-volume method. There, the rheology of the fluids has been modelled by the power-law able to describe the shear-thinning (pseudoplastic) behaviour of a series of polymer solutions. Numerical simulation based on finite element method for general Newtonian has been conducted by Mitsoulis and Kotsos [10]. In this study, the Herschel-Bulkley constitutive model is implemented, which reduces to the Newtonian, power-law and Bingham, models. Belblidia et al. [2] used a Taylor-Galerkin/pressure-correction to address the inelastic die-swell flows under two assumptions ; incompressible and compressible presentation. Wahba [11] used the power-law model to investigate shear-thinning and shear-thickening effects of fluid on the transient flow behavior.

Numerically, Galerkin finite element approach is implemented to solve the governing equations of incompressible general Newtonian flow in cylindrical coordinates [12]. Our previous studies have mostly focused primarily on the steady state flow of Newtonian fluids through straight channel, and have not investigated how general Newtonian features influence flow behavior (see [1]).

The present study aims to present a study on the incompressible power-low inelastic fluid with a viscosity dependent on simple shear-rate. The novelty here is to study the temporal convergence-rate of the system solution that is taken to be steady state, incompressible, axisymmetric, and laminar, which did not address by researchers previously. In this context, Poiseuille(Ps) flow along a two dimensional planar straight channel, under isothermal condition is studied. The main results of current study focused on the convergence rate of velocity and pressure solutions under the variation of power low parameters and Reynolds number presented. Furthermore, determination of the critical levels of Reynolds number (Re) is also reoresented the excited issue of this study. Numerical treatments are presented for governing system, where we are utilzed the Galerkin finite element method (GFEM).

2 Mathematical modelling

For inelastic (non-Newtonian) constitutive modelling, the extra stress tensor may be reforested as

$$T = 2\mu(\dot{\gamma}, \dot{\varepsilon})d, \tag{1}$$

where, $\dot{\gamma}$, $\dot{\varepsilon}$ represent shear-rate and strain-rate for simple shear flow and extensional flow, respectively, and d is the deformation rate of the fluid, such that

$$\dot{\gamma} = 2\sqrt{II_d}, \tag{2}$$

$$\dot{\varepsilon} = 3\frac{III_d}{II_d}, \tag{3}$$

$$d = \frac{1}{2}(\nabla u + \nabla u^T). \tag{4}$$

Here, II_d and III_d represent the second and third invariants of the rate of strain tensor d which, in axisymmetric coordinate system can be defined as (see [5])

$$II_d = \frac{1}{2}tr(d^2) = \frac{1}{2}\{(\frac{\partial u_r}{\partial r})^2 + (\frac{\partial u_z}{\partial z})^2 + (\frac{u_r}{r})^2 + \frac{1}{2}(\frac{\partial u_r}{\partial z} + \frac{\partial u_z}{\partial r})^2\}, \tag{5}$$

and

$$III_d = det(d) = \frac{u_r}{r}\{\frac{\partial u_r}{\partial r}\frac{\partial u_z}{\partial z} - \frac{1}{4}(\frac{\partial u_r}{\partial z} + \frac{\partial u_z}{\partial r})^2\}. \tag{6}$$

Hence, for incompressible inelastic fluid flows under an isothermal setting, the governing equations may be expressed as:

$$\nabla \cdot u = 0, \tag{7}$$

$$\rho\frac{\partial u}{\partial t} = \nabla \cdot (2\mu(\dot{\gamma}, \dot{\varepsilon})d) - \rho(u \cdot \nabla u) - \nabla p. \tag{8}$$

Here, for inelastic fluids the viscosity is a function of combined shear-rate and extension–rate. Also, p is the pressure and ρ is the density of the fluid . In the cylindrical coordinates the continuity equation for conservation of mass and time-dependent conservation of momentum equation are expressed as:

$$\frac{\partial u_r}{\partial r} + \frac{1}{r}u_r + \frac{1}{r}\frac{\partial u_\theta}{\partial \theta} + \frac{\partial u_z}{\partial z} = 0. \tag{9}$$

r-direction

$$\frac{\partial u_r}{\partial t} + u_r\frac{\partial u_r}{\partial r} + u_\theta(\frac{1}{r}\frac{u_r}{\partial \theta} - \frac{1}{r}u_\theta) + u_z\frac{\partial u_r}{\partial z} = \frac{-1}{\rho}\frac{\partial p}{\partial r} + \frac{2\mu_s}{\rho}\frac{\partial^2 u_r}{\partial r^2}$$
$$+ \frac{\mu_s}{\rho r^2}\frac{\partial^2 u_r}{\partial \theta^2} - \frac{\mu_s}{\rho r^2}\frac{\partial u_\theta}{\partial \theta} + \frac{2\mu_s}{\rho r}\frac{\partial u_r}{\partial r} + \frac{\mu_s}{\rho r}\frac{\partial^2 u_\theta}{\partial \theta \partial r} + \frac{\mu_s}{\rho}\frac{\partial^2 u_r}{\partial z^2} + \frac{\mu_s}{\rho}\frac{\partial^2 u_z}{\partial z \partial r}. \tag{10}$$

θ-direction

$$\frac{\partial u_\theta}{\partial t} + u_r\frac{\partial u_\theta}{\partial r} + u_\theta(\frac{1}{r}u_r + \frac{\partial u_\theta}{\partial \theta}) + u_z\frac{\partial u_\theta}{\partial z} = \frac{-1}{\rho r}\frac{\partial p}{\partial \theta} + \frac{2\mu_s}{\rho r^2}\frac{\partial u_r}{\partial \theta}$$
$$+ \frac{2\mu_s}{\rho r^2}\frac{\partial^2 u_\theta}{\partial \theta^2} + \frac{\mu_s}{\rho}\frac{\partial^2 u_\theta}{\partial r^2} + \frac{\mu_s}{\rho r}\frac{\partial^2 u_r}{\partial r \partial \theta} + \frac{\mu_s}{\rho}\frac{\partial^2 u_\theta}{\partial z^2} + \frac{\mu_s}{\rho r}\frac{\partial^2 u_z}{\partial z \partial \theta}. \tag{11}$$

z-direction

$$\frac{\partial u_z}{\partial t} + u_r \frac{\partial u_z}{\partial r} + u_\theta \frac{1}{r}\frac{\partial u_z}{\partial \theta} + u_z \frac{\partial u_z}{\partial z} = \frac{-1}{\rho}\frac{\partial p}{\partial z} + \frac{2\mu_s}{\rho}\frac{\partial^2 u_z}{\partial z^2}$$
$$+ \frac{\mu_s}{\rho}\frac{\partial^2 u_z}{\partial r^2} + \frac{\mu_s}{\rho r}\frac{\partial u_r}{\partial z} + \frac{\mu_s}{\rho r}\frac{\partial u_z}{\partial r} + \frac{\mu_s}{\rho}\frac{\partial^2 u_r}{\partial r \partial z} + \frac{\mu_s}{\rho r^2}\frac{\partial^2 u_z}{\partial \theta^2} + \frac{\mu_s}{\rho r}\frac{\partial^2 u_\theta}{\partial \theta \partial z}. \quad (12)$$

In contrast, the momentum equation (8) can be also defined by the non-dimensional groups of Reynolds number (Re), which is defined by the scales of velocity (U), length (L) and density (ρ) (for more details see ([12]-[15])). Thus, in this case the non-dimensional momentum equation for general Newtonian can be written as

$$Re\frac{\partial u}{\partial t} = \nabla \cdot (2\mu(\dot{\gamma}, \dot{\varepsilon})d) - Re(u \cdot \nabla u) - \nabla p. \quad (13)$$

3 Material modelling considerations

For non-Newtonian fluids, there are many possible inelastic constitutive models to consider. Some of these models describe shear viscous stress response and the others present extensional response. In addition, many materials are non-Newtonian, and exhibit either shear-thinning or shear-thickening behaviour.

The most fundamental constitutive model is that which describes shear viscous stress response of power-law form, which describes shear-thinning or shear-thickening behaviour. Fluids of this type, originally proposed by Ostwald-de Waele, may be expressed as:

$$\tau = (k|\dot{\gamma}|^{n-1})\dot{\gamma}, \quad (14)$$

where k is a consistency parameter and n is a power-law index. Then, higher k-values are found to exhibit more viscous fluid characteristics. When $n = 1$, the Newtonian limiting approximation is recovered, with no shear-rate dependence; shear thinning is gathered for $n < 1$ (as applied in this task) and shear-thickening is observed for $n > 1$.

4 The material functions of power low model

In this section the behaviour of the ($PLIM$) is presented to see the effect of n- variation and k-variation. The Newtonian and inelastic material functions are considered in Figure 1. In this Figure the viscosity is presented as a function of the shear rate ($\dot{\gamma}$), with $k = 1$ and n- variation. The constitutive model that describes shear viscous stress response of power-law form, which

describes shear-thinning or shear-thickening behaviour (see eq (14)). In this model k is a consistency parameter and n is a power-law index. Here one can see that, when $n = 1$, the Newtonian limiting approximation is recovered, with no shear-rate dependence; shear thinning is gathered for $n < 1$ and shear-thickening is observed for $n > 1$ (see Figure 1).

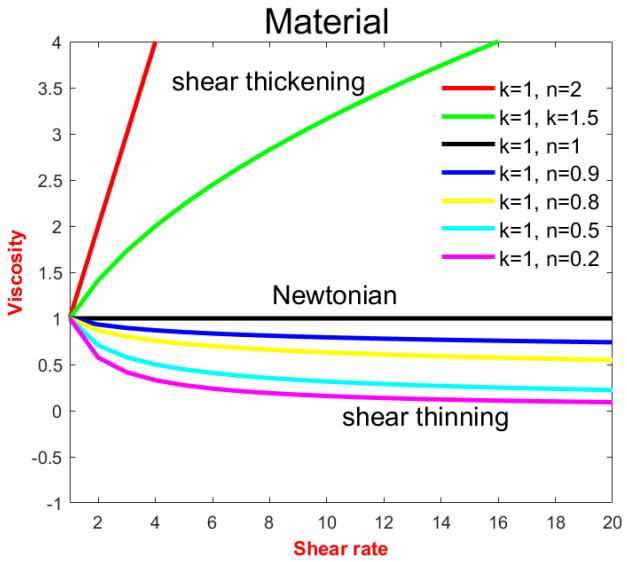

Figure 1: Material functions, Newtonian vs Inelastic, n-variation, $k = 1$.

Moreover, to see the behaviour of the model when the level of k is varied, the viscosity is plotted as a function of the shear rate for that sense (see Figure 2). The Figure shown that, higher k-values are found to exhibit more viscous fluid characteristics.

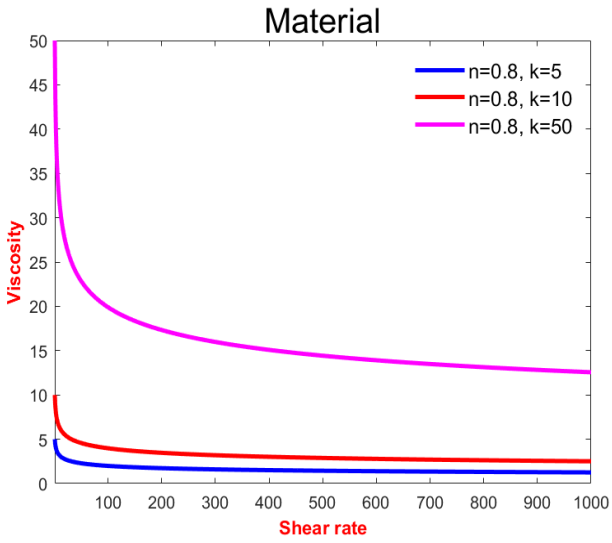

Figure 2: Material functions, Newtonian vs Inelastic, k-variation, n = 0.8.

5 Numerical method

The Calerkin finite element method is proposed to solve the system of equation (9)-(12). The main concept of this method is to find the weak form of the equation by using appropriate weight functions W and Q , such that the first function W for momentum equation and the second function Q for continuity equation. In addition, three quadratic shape functions of velocity components in cylindrical coordinates are utilized. These functions are given in natural coordinates as:

$$\begin{bmatrix}\psi_1\\ \psi_2\\ \psi_3\\ \psi_4\\ \psi_5\\ \psi_6\end{bmatrix} = \begin{bmatrix}L_1^2 - L_1(L_2+L_3)\\ L_2^2 - L_2(L_3+L_1)\\ L_3^2 - L_3(L_1+L_2)\\ 4L_1L_2\\ 4L_2L_3\\ 4L_3L_1\end{bmatrix} = \begin{bmatrix}1 & 0 & 0 & -1 & 0 & -1\\ 0 & 1 & 0 & -1 & -1 & 0\\ 0 & 0 & 1 & 0 & -1 & -1\\ 0 & 0 & 0 & 4 & 0 & 0\\ 0 & 0 & 0 & 0 & 4 & 0\\ 0 & 0 & 0 & 0 & 0 & 4\end{bmatrix}\begin{bmatrix}L_1^2\\ L_2^2\\ L_3^2\\ L_1L_2\\ L_2L_3\\ L_3L_1\end{bmatrix}. \tag{15}$$

In contrast, for pressure the following linear shape functions are employed:

$$\begin{bmatrix}\phi_1\\ \phi_2\\ \phi_3\end{bmatrix} = \begin{bmatrix}L_1\\ L_2\\ L_3\end{bmatrix}, \tag{16}$$

such that,

$$L_i = \frac{1}{2A_{area}}(a_i + b_i r + c_i z), \qquad (\forall i = 1,2,3).$$

where A_{area} is the area of the element's triangular and a_i, b_i, and c_i are coefficients. Thus from Gauss's theorem and rearranging the terms, we obtain the weak form of three dimensional Navier-Stokes equations as:

$$[Q_1^\tau][u_r] + [q][u_r] + [Q_2^\tau][u_\theta] + [Q_3^\tau][u_z] = 0, \tag{17}$$

$$[M][\dot{u}_r] + [C(u_r,u_\theta,u_z)][u_r] + [c_\theta][u_\theta] - \frac{1}{Re}[Q_1][p] + [K_{rr}][u_r] +$$

$$[K_{21}][u_\theta] + [K_{22}][u_r] + [k_r][u_r] + [k_\theta][u_\theta] + [K_{31}][u_z] + [K_{33}][u_r] = 0, \tag{18}$$

$$[M][\dot{u}_\theta] + [C(u_r,u_\theta,u_z)][u_\theta] + [c_r][u_r] - \frac{1}{Re}[Q_2][p] + [K_{11}][u_\theta] +$$

$$[K_{12}][u_r] - [k_\theta][u_r] + [K_{\theta\theta}][u_\theta] + [K_{33}][u_\theta] + [K_{32}][u_z] = 0, \tag{19}$$

$$[M][\dot{u}_z] + [C(u_r,u_\theta,u_z)][u_z] - \frac{1}{Re}[Q_3][p] + [K_{11}][u_z] + [K_{13}][u_r] -$$

$$[k_3][u_r] - [k_1][u_z] + [K_{22}][u_z] + [K_{23}][u_\theta] + [K_{zz}][u_z] = 0. \quad (20)$$

Consequentially, by using the theory of area coordinates for triangular elements, the mass matrix can be expressed as

$$[M] = \int_{\Omega^e} \psi\psi^\tau d\Omega = \int_{A^e} \int_0^{2\pi} [N][H][H^\tau][N^\tau] r d\theta dA = 2\pi \int_{A^e} [N][H][H^\tau][N^\tau] r dA,$$

where,

$$r_m = \frac{r_1+r_2+r_3}{3}, \qquad z_m = \frac{z_1+z_2+z_3}{3}.$$

Thus,[1]

$$[M] = 2\pi r_m [N]\underline{[H][H^\tau]}[N^\tau] \int_{A^e} dA = 2\pi r_m A_{area} [N]\underline{[H][H^\tau]}[N^\tau]. \quad (21)$$

Also, the derivative form of shape functions can be defined as

$$\frac{\partial\psi}{\partial r} = [N]\frac{\partial[H]}{\partial r} = [N][B][E],$$

$$\frac{\partial\psi}{\partial\theta} = 0,$$

$$\frac{\partial\psi}{\partial z} = [N]\frac{\partial[H]}{\partial z} = [N][C][E],$$

where,

$$[B] = \frac{1}{2A_{area}}\begin{bmatrix} 2b_1 & 0 & 0 \\ 0 & 2b_2 & 0 \\ 0 & 0 & 2b_3 \\ b_2 & b_1 & 0 \\ 0 & b_3 & b_2 \\ b_3 & 0 & b_1 \end{bmatrix}, [C] = \frac{1}{2A_{area}}\begin{bmatrix} 2c_1 & 0 & 0 \\ 0 & 2c_2 & 0 \\ 0 & 0 & 2c_3 \\ c_2 & c_1 & 0 \\ 0 & c_3 & c_2 \\ c_3 & 0 & c_1 \end{bmatrix}.$$

On the other hand, the final diffusion matrix formula can be written as

$$[K_{rr}] = 4\pi r_m A_{area} \frac{\beta}{Re} [N][B]\underline{[E][E^\tau]}[B^\tau][N^\tau], \quad (22)$$

$$[K_{zz}] = 4\pi r_m A_{area} \frac{\beta}{Re} [N][C]\underline{[E][E^\tau]}[C^\tau][N^\tau], \quad (23)$$

$$[K_{11}] = 2\pi r_m A_{area} \frac{\beta}{Re} [N][B]\underline{[E][E^\tau]}[B^\tau][N^\tau], \quad (24)$$

$$[K_{33}] = 2\pi r_m A_{area} \frac{\beta}{Re} [N][C]\underline{[E][E^\tau]}[C^\tau][N^\tau], \quad (25)$$

[1] $\underline{[\,]}$: Underline symbol refers to the evaluation of matrix at the centroid.

$$[K_{13}] = 2\pi r_m A_{area} \frac{\beta}{Re} [N][B]\underline{[E][E^\tau]}[C^\tau][N^\tau], \quad (26)$$

$$[K_{31}] = 2\pi r_m A_{area} \frac{\beta}{Re} [N][C]\underline{[E][E^\tau]}[B^\tau][N^\tau], \quad (27)$$

$$[k_r] = 4\pi A_{area} \frac{\beta}{Re} [N]\underline{[H][E^\tau]}[B^\tau][N^\tau], \quad (28)$$

$$[k_1] = 2\pi A_{area} \frac{\beta}{Re} [N]\underline{[H][E^\tau]}[B^\tau][N^\tau], \quad (29)$$

$$[k_3] = 2\pi A_{area} \frac{\beta}{Re} [N]\underline{[H][E^\tau]}[C^\tau][N^\tau], \quad (30)$$

$[K_{\theta\theta}] = 0$, $[K_{22}] = 0$, $[K_{12}] = 0$, $[K_{21}] = 0$, $[K_{23}] = 0$, $[K_{32}] = 0$, $[k_2] = 0$, $[k_\theta] = 0$.

Moreover, the gradient matrix is defined as

$$[Q_1] = 2\pi r_m A_{area}[N][B]\underline{[E][E^\tau]}, \quad (31)$$

$$[Q_3] = 2\pi r_m A_{area}[N][C]\underline{[E][E^\tau]}, \quad (32)$$

$$[q] = 2\pi A_{area}\underline{[E][H^\tau]}[N^\tau], \quad (33)$$

$$[Q_2] = 0.$$

Finally, the convective matrix is given by

$$[C_r(u_r)] = 2\pi r_m A_{area}[N]\underline{[H][H^\tau]}[N^\tau][u_r]\underline{[E^\tau]}[B^\tau][N^\tau], \quad (34)$$

$$[C_z(u_z)] = 2\pi r_m A_{area}[N]\underline{[H][H^\tau]}[N^\tau][u_z]\underline{[E^\tau]}[C^\tau][N^\tau], \quad (35)$$

$$[c_\theta] = -2\pi A_{area}[N]\underline{[H][H^\tau]}[N^\tau][u_\theta]\underline{[H^\tau]}[N^\tau], \quad (36)$$

$$[c_r] = 2\pi A_{area}[N]\underline{[H][H^\tau]}[N^\tau][u_\theta]\underline{[H^\tau]}[N^\tau], \quad (37)$$

$$[C_\theta(u_\theta)] = 0.$$

As it is known the real challenge in the present problem lies non-linear term, which needs efficient treatment. So, to address this non-linear term of equation (17)-(20), the Newton-Raphson approach is achieved . As the result, the system of equation will be replaced by the following equation:

$$\begin{bmatrix} M & 0 & 0 & 0 \\ 0 & M & 0 & 0 \\ 0 & 0 & M & 0 \\ 0 & 0 & 0 & 0 \end{bmatrix} \begin{bmatrix} \dot{u}_r \\ \dot{u}_\theta \\ \dot{u}_z \\ \dot{p} \end{bmatrix} + \begin{bmatrix} \frac{\partial R_1}{\partial u_r} & \frac{\partial R_1}{\partial u_\theta} & \frac{\partial R_1}{\partial u_z} & \frac{\partial R_1}{\partial p} \\ \frac{\partial R_2}{\partial u_r} & \frac{\partial R_2}{\partial u_\theta} & \frac{\partial R_2}{\partial u_z} & \frac{\partial R_2}{\partial p} \\ \frac{\partial R_3}{\partial u_r} & \frac{\partial R_3}{\partial u_\theta} & \frac{\partial R_3}{\partial u_z} & \frac{\partial R_3}{\partial p} \\ \frac{\partial R_4}{\partial u_r} & \frac{\partial R_4}{\partial u_\theta} & \frac{\partial R_4}{\partial u_z} & \frac{\partial R_4}{\partial p} \end{bmatrix} \begin{bmatrix} u_r^{n+1} - u_r^n \\ u_\theta^{n+1} - u_\theta^n \\ u_z^{n+1} - u_z^n \\ p^{n+1} - p^n \end{bmatrix} = - \begin{bmatrix} R_1 \\ R_2 \\ R_3 \\ R_4 \end{bmatrix}. \quad (38)$$

or

$$[M]\dot{U} + [S(U)]\Delta U = -[R]. \quad (39)$$

6 Problem specification

Poiseuille (Ps) flow through a $2D$ axisymmetric straight channel is introduced in this study under isothermal condition. For this context, two different triangular finite element meshes are implemented, 2×2 and 5×5 as shown in Figure 3 , with connectivities structure. In addition, the mesh characteristics are introduced in Table 1.

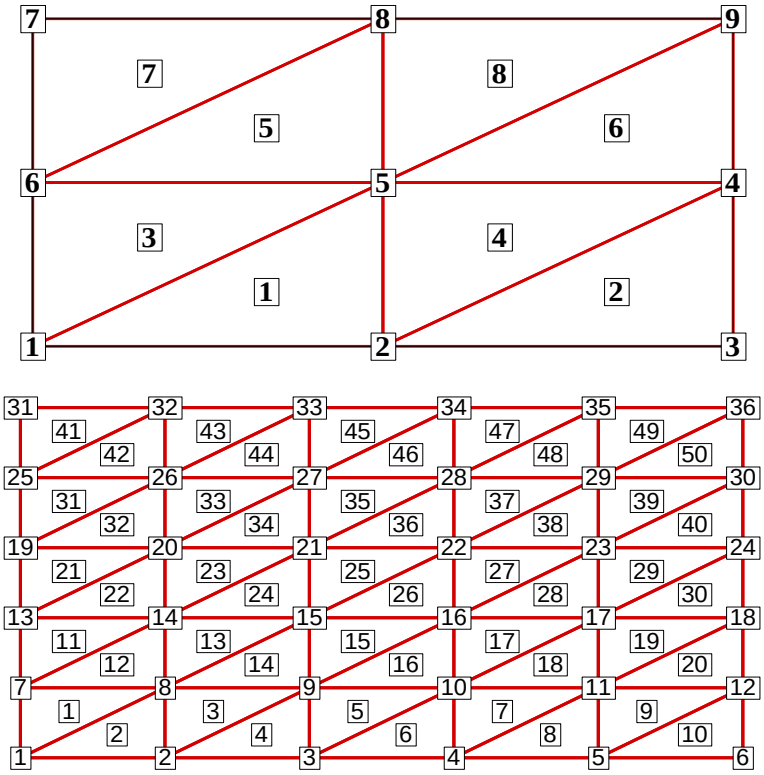

Figure 3: Structured 2×2 and 5×5 finite element meshes.

Table 1: Mesh characteristic parameters.

Mesh	Total Element	Total Nodes	Boundary Nodes	Pressure Nodes
2×2	8	25	16	9
5×5	50	121	40	36

Boundary conditions (BCs): The setting of BC_s of the present channel problem is laid as follows (see Figure 4):

(1) Poiseuille (Ps) flow is specified at the inlet with zero radial velocity .

(2) No-slip BCs is applied on the top and bottom walls of the channels.

(3) Zero radial velocity applies and zero pressure are applied on the outlet of the channels.

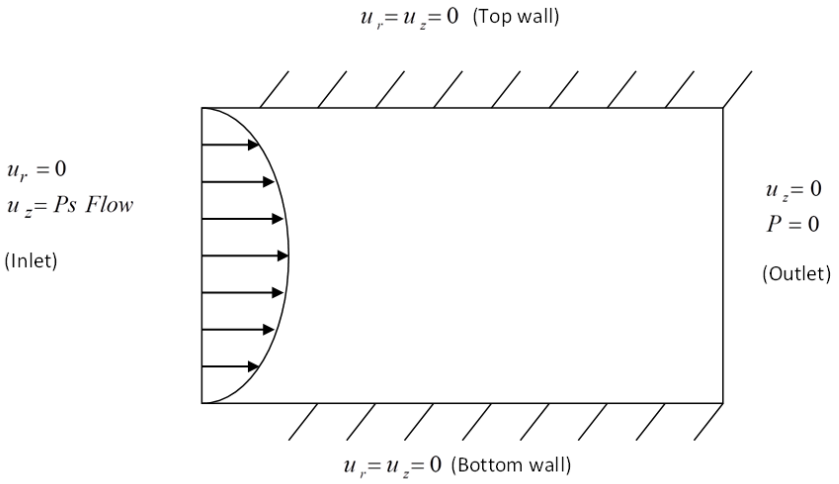

Figure 4: Schema for flow problem, boundary conditions.

7 Numerical results

The numerical results concerned with the rate of error convergence of the problem under consideration by using Galerkin finite element method. Here the effect of power-law index (n), consistency parameter (k) and Reynolds number (Re) on the numerical convergence is investigated.

***n*-variation**:The rate of convergence for axial velocity and pressure components are pressented in Figure 5, with Re=0.001, $k = 1$ and different values of the power-law index n ($n =$ 1,0.8,0.6,0.4,0.2). The results reveal that, the level of velocity convergence have been incresesed as the valuse of power-law index (n) decreased (see Figure 5a) due to the shear thinning behaviours. In content and from Figure5b one can observe that there is no significant change in the level of convergence of pressure at the same setting of the power-law index (n). Figure 5c shown that the level of convergence for velocity component is higher compared to pressure because of the influence of non-linearity behaviour.

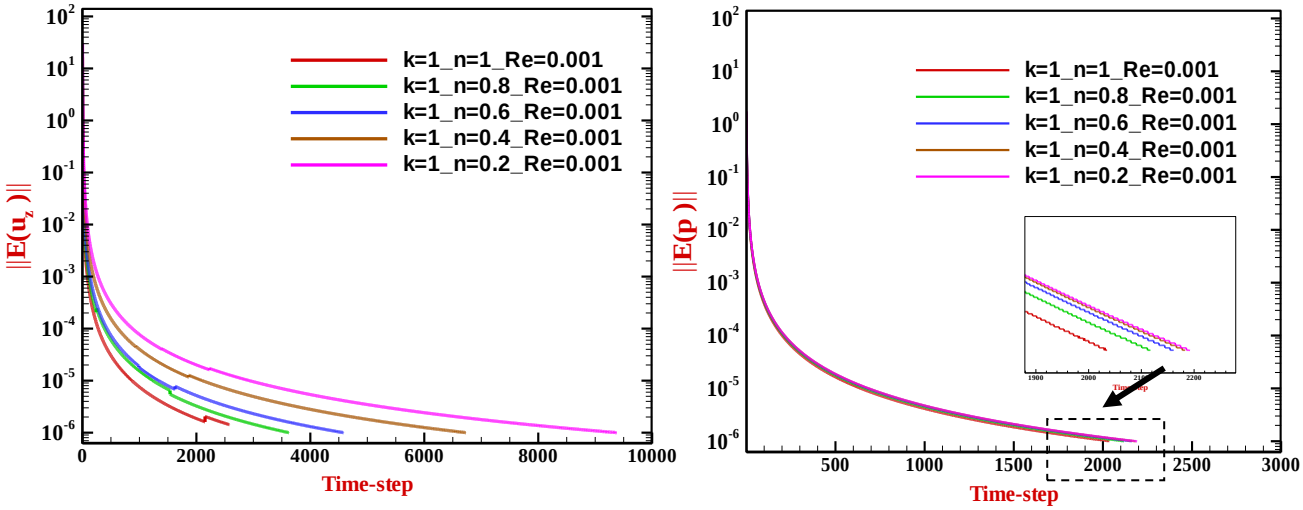

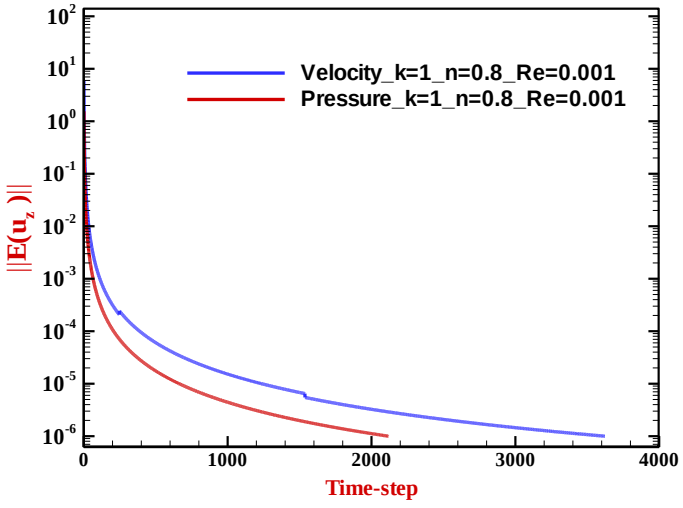

Figure 5: Convergence of velocity and pressure; n -various, $k = 1$, $Re = 0.001$.

***k*-variation**: Opposite feature have been observed in the study of k-variation under fixed $n = 0.8$ and fixed $Re = 0.001$. Here, the level of convergence for velocity and pressure almost closed for all value of k. The interesting thing in the results is that the level of convergence in the k-variation is almost double compared to the case of n-variation (compare Figure 5 and Figure 6).). For more detail comparison between the error and CPU time is provided in Table 2 in axial velocity.

Table 2: Comparison of error and CPU time ; n-various , k=1, Re=0.001.

		Time					
n-variation	Error	0.2	0.5	0.8	5	15	25
1	$\|u_z\|_{L_2}$	1.8×10^{-2}	3×10^{-3}	1.2×10^{-3}	3.04×10^{-5}	3.3×10^{-6}	1.52×10^{-7}
	CPU(s)	1.0141	2.0449	2.5226	11.3739	32.0353	52.3288
0.8	$\|u_z\|_{L_2}$	2.9×10^{-2}	4.9×10^{-3}	1.9×10^{-3}	6.05×10^{-4}	6.8×10^{-6}	2.09×10^{-7}
	CPU(s)	1.1666	2.1067	2.6336	11.4011	32.1872	52.5862
0.6	$\|u_z\|_{L_2}$	4.2×10^{-2}	7×10^{-3}	2.7×10^{-3}	7.4×10^{-5}	7.9×10^{-6}	3.32×10^{-7}
	CPU(s)	1.4285	2.3532	3.0728	11.5236	32.8504	52.9282

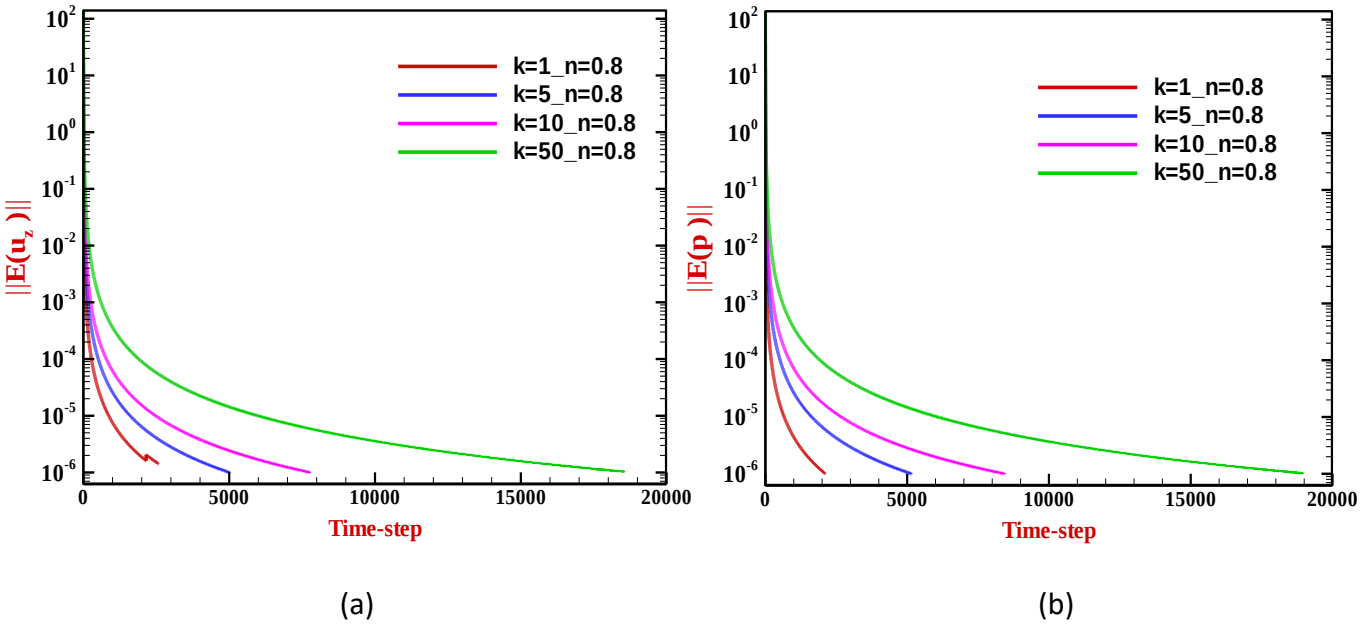

(a) (b)

Figure 6: Convergence of velocity and pressure; k-various, n=0.8, Re=0.001.

***Re*-variation**:Figure 7 illustrates the convergence of the axial velocity through variation in Reynolds number (Re) at fixed n-value (n=0.8) and k-value (k=1). The finding reflects the effect of Re on the level of convergence, where that level is high with high Re. In addition we found out that the critical value of Re under the inelastic assumption is 1.

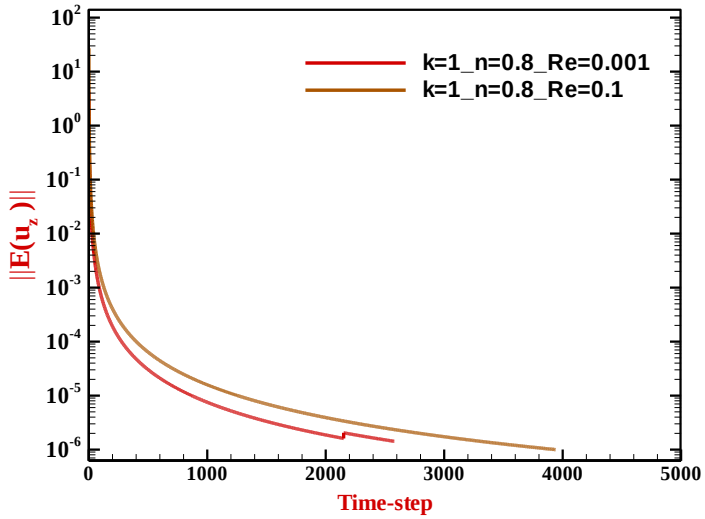

Figure 7: Convergence of axial velocity; Re-various, n=0.8, k=1.

Cross-channel velocity profiles in radial and axial component forms are provided in Figure 8 at fixed n (n=0.5), k (k=1) and Re=0.001. The axial velocity profile shows parabolic flow structure for $0 \leq z \leq 2$, where a Poiseuille flow is appeared over this zone. Along the axial span $0 \leq z \leq 2$, the axial velocity decreases as z increases, where a maxima at $z \leq 0$ reduce by almost 0.8 unit at z= -0.5 to 2.

[2] $\|\|_{L_2}$: norm over L_2 (least square measure)

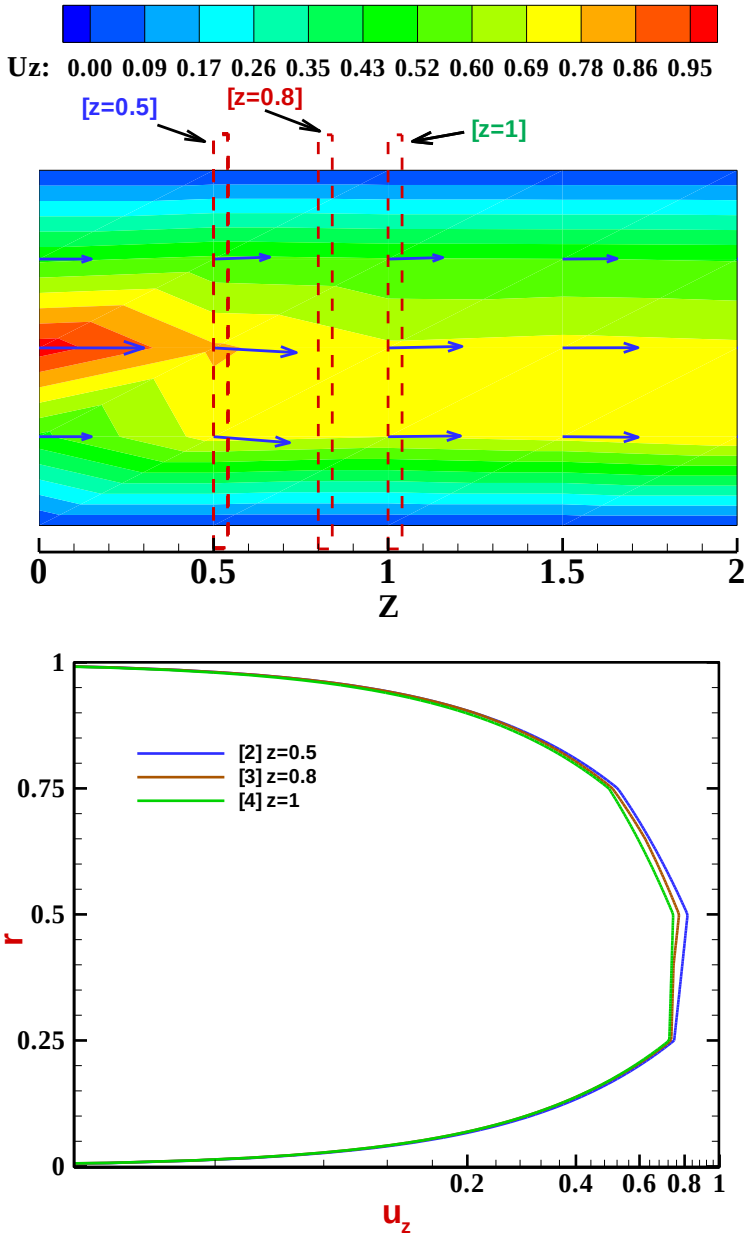

Figure 8: Cross-channel axial velocity field and profile: n =0.5, k =1, Re=0.001.

8 Conclusion

In this study, the numerical simulation for incompressible power-low inelastic fluid is conducted based on the Galerkin finite element method. The power-law model in shear-thinning response is used to describe shear viscous stress. The effect of a consistency parameter (k) and a power-law

index (n) are shown in this investigation. In addition the level of Reynolds number (Re) under k-variation and n-variation is considered as well.

The convergence analysis of velocity and pressure was done to identify the effect of k, n and Re on the acceleration of convergence. From the results one can observe that, the rate of convergence of velocity is increased as power-law index (n) decreased, whereas an opposite feature is appeared with the a consistency parameters (k) and (Re) . In contrast, less significant is observed for isotropic pressure.

References

[1] B .K. Jassim, A .H. Al-Muslimawi, Numerical analysis of Newtonian flows based on artificial compressibility AC method.*Journal of Al-Qadisiyah for computer science and mathematics*. **9** (2017) 115-128.

[2] F. Belblidia, T. Haroon, M. F. Webster, The Dynamics of Compressible Herschel-Bulkley Fluids in Die-Swell Flows, *In Damage and Fracture Mechanics.* (2009) 425-434. Springer, Dordrecht.

[3] F. H. Norton, *The creep of steel at high temperatures* (No. 35), McGraw-Hill Book Company, Incorporated. (1929).

[4]]N. J. Hoff, Approximate analysis of structures in the presence of moderately large creep deformations, *Quarterly of Applied Mathematics*, **12** (1954) 49-55.

[5] A. H. A. Al-Muslimawi, *Numerical analysis of partial differential equations for viscoelastic and free surface flows*, (Doctoral dissertation, Swansea University),(2013).

[6] R. B. Bird, Armstrong, R.C. and Hassager, O. *Dynamics of polymeric liquids. Vol. 1: Fluid mechanics.*(1987).

[7] P. J. Carreau, Rheology of polymeric systems: principles and applications. (1997)

[8] S. H. Garrioch, D. F. James, A finite-element study of Newtonian and power-law fluids in conical channel flow, Journal of fluids engineering 119.2 (1997) 341-346.

[9] K. A. Missirlis, Assimacopoulos, D., Mitsoulis, E. and Chhabra, R.P., Wall effects for motion of spheres in power-law fluids, *Journal of Non-Newtonian Fluid Mechanics*, **96** (2001), 459-471.

[10] E. Mitsoulis, P. Kotsos, Numerical simulation of wire coating pseudoplastic and viscoplastic fluids. In Advanced Methods in Material Forming, Springer, Berlin, Heidelberg. (2007) 279-295.

[11] E. M. Wahba, Non-Newtonian fluid hammer in elastic circular pipes: Shear-thinning and

shear-thickening effects. *Journal of Non-Newtonian Fluid Mechanics*, **198** (2013) 24-30.

[12] A. J. Davies, The finite element method: An introduction with partial differential equations, OUP Oxford (2011).

[13] A. Al-Muslimawi, H. R. Tamaddon-Jahromi, M. F. Webster, Numerical simulation of tube-tooling cable-coating with polymer melts, *Korea-Australia Rheology Journal*, **25** (2013), 197-216.

[14] J. E. López-Aguilar, M. F. Webster, A. H. A. Al-Muslimawi, H. R. Tamaddon-Jahromi, R. Williams, K. Hawkins, C. Askill, C. L. Ch'ng, G. Davies, P. Ebden, K. Lewis, A computational extensional rheology study of two biofluid systems, Rheologica Acta, **54** (2015) 287-305.

[15]] A. H. Al-Muslimawi, Taylor Galerkin Pressure Correction (TGPC) Finite Element Method for Incompressible Newtonian Cable-Coating Flows, *Journal of Kufa for Mathematics and Computer*. **5** (2018) 13-21.

المحاكاة العددية للسوائل غير المرنة في قانون الطاقة باستخدام طريقة العناصر المحدودة

ريسان ياسين ياسر، علاء حسن المسلماوي
قسم الرياضيات ، كلية العلوم ، جامعة البصرة

المستخلص

في هذه البحث ، تم تقديم الدراسة العددية للسائل غير المرن المنخفض الطاقة غير القابل للضغط ، حيث يتم استخدام معادلة الاستمرارية (الحفظ الشامل) والحفظ المعتمد على الوقت لمعادلات الزخم لوصف حركة السائل. علاوة على ذلك ، تم حل مشكلة التدفق تحت افتراضات غير مرنة لزجة ، مع نموذج مرن لقانون الطاقة (PLIM) من الناحية العددية، أجريت الدراسة على أساس طريقة العناصر المحددة (GFEM). ركزت الدراسة على المقارنة بين النتائج النيوتونية وغير المرنة لتخفيف القص.

تم إجراء تحليل التقارب وفقًا معلمات نموذج الطاقة المرنة منخفضة الطاقة وعدد رينولدز. النتائج اوضحت أن هناك تأثيرًا كبيرًا من المعلمات غير المرنة على معدلات التقارب الزمني للسرعة ، بينما بالنسبة إلى الضغط ، فإن التغيير في التقارب بسيط.